

# Outer Shell Type 2 DOF Bending Manipulator using Spring-link Mechanism for Medical Applications

Jumpei Arata, Yoshitaka Saito and Hideo Fujimoto

**Abstract**— In recent years, robotic technology has been introduced to medical fields and many surgical robots have been presented not only in academic fields but also as commercialized products. In this paper, an outer shell type 2 DOF bending manipulator using a spring-link mechanism is presented. The mechanism was developed for a surgical robot, which can implement various surgical treatment devices inside of the manipulator. The spring-link mechanism is a simple combination of a flat spring and a rigid link with a passive joint connection. The outer shell type 2 DOF bending manipulator is composed by four spring-link mechanisms. The most unique feature of the manipulator is that these four springs are interconnected in the kinematics. Therefore, it is possible to realize a robust and backlash-free motion by taking into account the interconnections of springs such as an internal stress of the structure. In addition, by locating four spring-link mechanisms around the manipulator, it is possible to place medical devices inside of the manipulator.

## I. INTRODUCTION

In recent years, robotic technology has been introduced to medical fields and many surgical robots have been presented not only in academic fields but also as commercialized products[1]. One of the most advantageous features of these surgical robots is a dexterous motion in their miniature size. By realizing the complex motions on the tip of surgical tools, it is possible to introduce these surgical robots into patient body to achieve Minimally Invasive Surgery (MIS). For a successful example, the master-slave technology was effectively introduced to the applications of MIS in Da Vinci system[2]. In these backgrounds, many dexterous and miniature surgical robots have been developed. Ikuta, et al. presented a wire driven multi-DOF forceps[3]. Dario, et al. presented a new mechatronic tool for computer assisted arthroscopy using a wire driven mechanism[4]. Harada, et al. realized a 2 DOF bending laser manipulator of 2.4 mm diameter by using a wire driven mechanism[5]. And many wire driven mechanism were presented in past studies[6]-[12]. As a link driven mechanism, Merlet presented a micro parallel robot for MIS[13]. Yamashtia, et al. proposed a slider linkage mechanism for an endoscopic forceps manipulator[14]. The author presented a link driven multiple DOF forceps[15].

These previously presented robots can be mainly classified as wire mechanism and link mechanism. The wire mechanism has an advantage on miniaturization in multi-DOF structures. However, there are extension, friction and cutting problems as main drawbacks in using the wire mechanism. On the other hand, rigidity and durability can be obtained by

J. Arata is with Department of Computer Science and Engineering, Graduate School of Engineering, Nagoya Institute of Technology, Gokisocho, Showa-ku, Nagoya 466-8555, Japan. jumpei@nitech.ac.jp

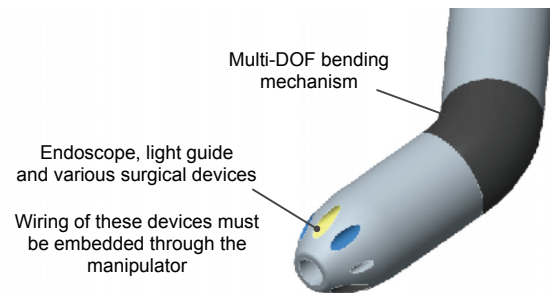


Fig. 1. Concept of a multi-tool equipped surgical robot

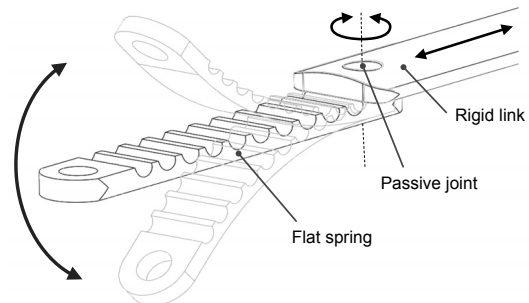


Fig. 2. Spring-link mechanism

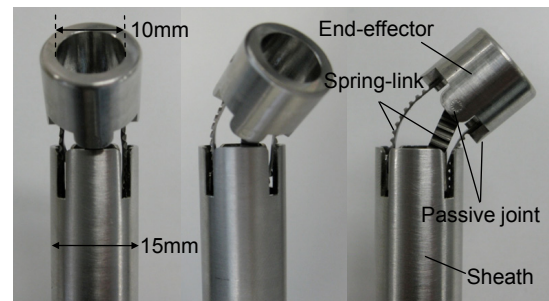


Fig. 3. Prototype of outer shell type 2 DOF bending manipulator using spring-link mechanism

introducing the rigid link mechanism, however, the structure requires usually a large number of mechanical components, which can be drawbacks on a cost issue, miniaturization and sterilization. Therefore, a new mechanism which can realize advantageous features of both wire and rigid link mechanisms is desired. In addition, various surgical treatment devices (not only a gripper, but also an endoscope, a light guide, an electric knife, and other advanced medical devices) are expected to be implemented on the tip of surgical robot for realizing more complex surgical procedures (Fig.1). For realizing such a multi-tool device, an outer shell type mechanism will be beneficial for putting these devices inside

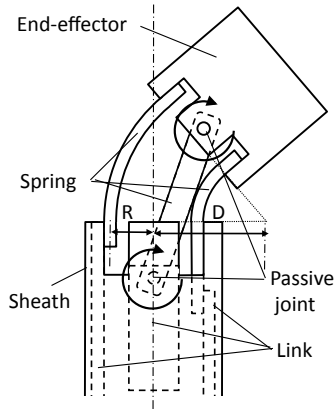


Fig. 4. Bending mechanism of the manipulator

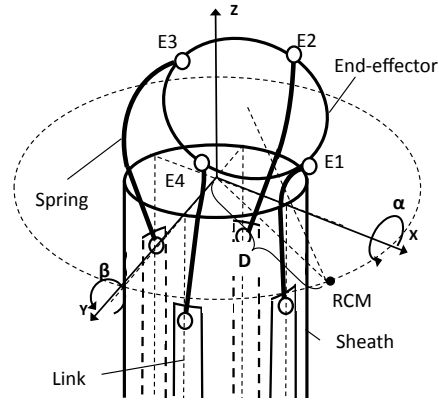


Fig. 5. Kinematic model of the manipulator

of the mechanism. Moreover, with the recent advancement of medical imaging technology, image-guided surgery using CT and/or MRI is becoming common. In introducing surgical robots into the image-guided surgery, the position accuracy is getting more important.

In this paper, an outer shell type 2 DOF bending manipulator using spring-link mechanism is presented. The spring-link mechanism is a simple combination of a flat spring and a rigid link with a passive joint connection. The outer shell bending manipulator is composed by four spring-link mechanisms. The most unique feature of the manipulator is that these four springs are interconnected and interact regarding the kinematics of manipulator. Therefore, it is possible to realize a robust and backlash-free motion by taking into account the interconnections of springs such as an internal stress of the structure. In addition, by locating four spring-link mechanism around the manipulator, it is possible to place medical devices inside of the manipulator.

The kinematics of the developed manipulator using the spring-link mechanism is presented in chapter II. The prototype implementation and evaluations are described in chapter III. A kinematic re-modeling for improvement of accuracy is described in chapter IV. Finally, the conclusions of this paper are given in chapter V.

## II. KINEMATICS

### A. Spring-link mechanism

The spring-link mechanism (**Fig.2**) is a simple combination of a flat spring and a rigid link with a passive joint connection. These advantages below can be obtained by introducing the spring-link mechanism into a manipulator.

- The interconnections of springs can be beneficial in terms of robustness and accuracy of manipulator.
- Internal space can be obtained by locating the mechanism around the manipulator.
- Smooth bending shape of springs can prevent the damage of surrounding environment.

The mechanism is exposed in the prototype presented in the paper for conducting evaluations. However, a further clinical-use prototype will be covered by a tube to prevent the damage to surrounding tissues.

### B. Kinematic model of the outer shell type 2 DOF bending manipulator

The outer shell type 2 DOF bending manipulator (**Fig.3**) realizes 2 DOF bending motions by two pairs of spring-link mechanisms, which are located in face-to-face in each pair (**Fig.4**). In this manipulator, a bending motion can be given by the bending motions of each pair of springs, which are driven by differential motions of the attached rigid links. **Fig.5** shows the kinematic model of the manipulator. In this mechanism, the bending motion of a pair of spring-link mechanisms affects on the other pair of spring-link mechanisms. However, the effect can be compensated by the passive joint, which connects between the spring and the rigid link. Consequently, it is possible to control the 2 DOF bending motions independently. Each pair of spring-link mechanisms has 2 DOF of linear motions of the rigid links. Therefore, the mechanism requires 4 DOF of linear actuators in total, and has redundancy in terms of the 2 DOF bending motions. The redundancy is used for determining the center of bending motion in terms of the axial and radial axis of the manipulator. For example, in the case where the all rigid links move in a same direction, the center of bending motions moves in the long axis. On the other hand, the rate of differential motions of a pair of rigid links determines the center of rotation in the radial axis. Therefore, it is possible to realize a smooth and compact bending motion by determining the appropriate kinematic parameters.

For the inverse kinematic model of manipulator, first, the input end-effector posture is described in Eulerian coordinates by using the bending angles  $\alpha$  and  $\beta$ .

$$\phi = \arcsin(\cos \alpha \cos \beta) \quad (1)$$

$$\theta = \begin{cases} \arcsin\left(\frac{-\cos \beta \sin \alpha}{\cos \phi}\right) & (\beta \geq 0) \\ \arcsin\left(\frac{-\cos \beta \sin \alpha}{\cos \phi}\right) + \pi & (\beta < 0) \end{cases} \quad (2)$$

By the homogeneous transformation matrix  ${}^0_5T$ , the coordinates of the center of end-effector can be obtained as:

$$\begin{aligned} {}^0_5T &= {}^0_1T_r(\mathbf{Z}, \theta) \cdot {}^1_2T_r(\mathbf{Y}, \left(\frac{\pi}{4} - \frac{\phi}{2}\right)) \\ &\quad \cdot {}^2_3T_t(2D \cos\left(\frac{\pi}{4} + \frac{\phi}{2}\right), 0, 0) \end{aligned}$$

TABLE I  
MOTOR SPECIFICATIONS

Model	Maxon EC22 20W
Motor diameter	$\phi 22$ mm
Length	82.8 mm
Speed at max continuous torque	16500 rpm
Max continuous torque	16.9 mN-m
Max continuous current	1.51 A

TABLE II  
BALL SCREW SPECIFICATIONS

Model	THK MDK0401-3
Outside diameter of thread	4 mm
Lead	1 mm
Length	64 mm
Basic static load rating	0.29 kN

$$\cdot {}_4^3T_r(\mathbf{Y}, \left(\frac{3}{4}\pi - \frac{\phi}{2}\right)) \cdot {}_5^4T_r(\mathbf{Z}, -\theta) \quad (3)$$

$$\begin{pmatrix} E_{0x} \\ E_{0y} \\ E_{0z} \end{pmatrix} = \begin{pmatrix} -D \cos \theta (-1 + \sin \phi) \\ -D \sin \theta (-1 + \sin \phi) \\ D \cos \phi \end{pmatrix} \quad (4)$$

$D$  is the radius of bending curvature,  $T_r$  is the rotation of each axis, and  $T_t$  is the translation of each axis.

From the coordinates of center of end-effector, the positions of passive joints  $E_{1-4}$ , which are connecting between the end-effector and four spring-link mechanisms, can be obtained. By assuming the deformation of spring as a circular arc as illustrated in **Fig.4**, the equations of linear link motions  $L_{1-4}$  can be obtained. Thus, the inverse kinematic model of manipulator can be obtained as following equations:

$$L_1 = \frac{L_a - E_{1z}}{\sqrt{(L_a + B(E_{1x} - R))^2 - E_{1y}^2}} \quad (5)$$

$$L_2 = \frac{L_a - E_{2z}}{\sqrt{(L_a + A(E_{2y} - R))^2 - E_{2x}^2}} \quad (6)$$

$$L_3 = \frac{L_a - E_{3z}}{\sqrt{(L_a + B(E_{3x} + R))^2 - E_{3y}^2}} \quad (7)$$

$$L_4 = \frac{L_a - E_{4z}}{\sqrt{(L_a + A(E_{4y} + R))^2 - E_{4x}^2}} \quad (8)$$

$$A = \left(\frac{\alpha - \sin \alpha}{1 - \cos \alpha}\right) \quad B = \left(\frac{\beta - \sin \beta}{1 - \cos \beta}\right) \quad (9)$$

$R$  is the distance between the long axis of manipulator and a spring.  $L_a$  is the length of springs.

### III. PROTOTYPE IMPLEMENTATION AND EVALUATION

The overview of prototype is shown in **Fig.6**. As the material of springs, super-elastic alloy (Ni-Ti) was used. The rigid links and other mechanical parts were fabricated from stainless steel. The diameter of the tip of manipulator is 15 mm, and the diameter of the internal cavity is 10 mm. The thickness of the robot is 2.5 mm in this implementation. The size of robot can be modified up to the devices to be

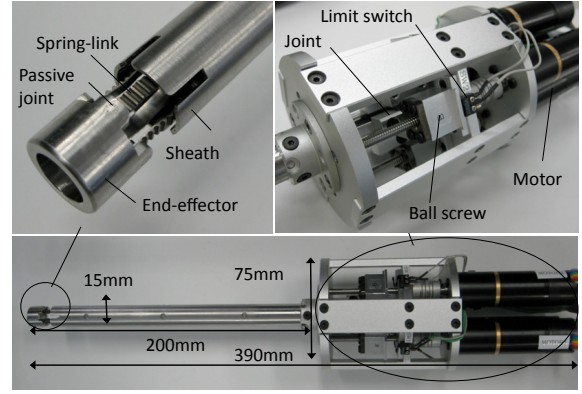


Fig. 6. Overview of the prototype

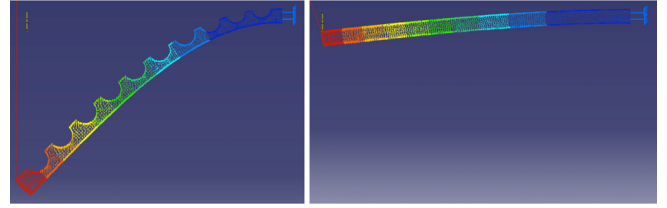


Fig. 7. Results of FEM analysis (left: with slits, right: without slits)

implemented in the internal cavity. The working area of the bending motions ( $\alpha$  and  $\beta$ ) are  $\pm 45$  deg, and it is adjustable by an implementation of longer springs on the mechanism (14 mm in this implementation, and longer springs can give a wider working area of bending angles). Four spring-link mechanisms are driven by DC servo motors and ball screws, which are connected by couplings. The specification of these mechanical components are described in **Table I** and **II**.

#### A. FEM analysis for spring design

For developing the spring-link mechanism, the characteristic of springs is important. The springs must be bend in a range of elastic deformation for preventing a breakage. Therefore, round shape slits were fabricated on the surface of springs for a wide range of elastic deformation. The dimensions of slits are 1.0 mm of diameter, 1.4 mm of pitch and 0.5 mm of depth from the surface of spring. By conducting FEM analysis in trying many patterns of slits, the design parameters were determined. **Fig.7** shows a deformation of a spring in applying a load on the tip of spring. Comparing with a spring without slits, the deformation can be seen clearly in a round shape in the case that the spring has slits. In this implementation, the mechanical design was given in a trial, and further analysis is on-going work for an optimal design.

#### B. Accuracy test

To test the accuracy of manipulator, a sine curve (amplitude: $\pm 30$  deg, cycle:20 s) was given as the bending angle order, then the positions of motors are controlled by using the inverse kinematic model. The position of manipulator was measured by using a 3D position sensor, Optotrak (Northern Digital Inc.) for the evaluation. The accuracy of Optotrak is 0.1 mm of RMS positional accuracy, and 0.01 mm of resolution. The manipulator was controlled

by using VxWorks 5.5.1 at a control frequency of 1 kHz. The experimental setup is shown in Fig.8. The measurement was conducted in  $\alpha$  and  $\beta$  axes independently. As the end-effector is supported by bending springs, the manipulator naturally has a shift of axial center by its interconnected structure. However, it is confirmed that the axial center shift has accurate repeatability by trial experiments. Therefore, the accuracy was evaluated by measuring the bending angles  $\alpha$  and  $\beta$ .

Fig.9 shows the experimental result of accuracy test in  $\alpha$  axis. From the result, it was observed that the bending angle of manipulator was smaller than it was expected from the kinematic model. The error was observed in maximum 2.3 deg on the peak of trajectory. This error was observed both in  $\alpha$  and  $\beta$  axes. On the other hand, the average error of repeat motions of  $\alpha$  and  $\beta$  axes was 0.010 deg and the maximum error was 0.031 deg. The result shows the high accuracy on repeat motions, however, the absolute position error was large. The error cause and the improvement of accuracy are discussed in the chapter IV.

### C. Rigidity test

The rigidity of the manipulator was measured by applying a load on the tip of manipulator. Then the displacement of the tip of manipulator was measured by using Optotrak in the same experimental setup as the accuracy test. The bending angle ( $\alpha$  axis) was varied from 0 to 30 deg in every 10 deg. The load was gradually applied from 0 to 5 N in every 0.5 N, and unloaded from 5 to 0 N in the same manner. The load was applied directly to the bending direction. From the experimental result (Fig.10), the average of rigidity was 27.95 N/mm. The experimental result revealed a high rigidity of the manipulator. In addition, rigidity was getting higher in increasing the bending angle. This can be considered as the effect of spring components. In increasing the bending angle, the pair of springs was bended in sharper angles. Therefore, the internal force of the mechanism was increased, eventually, the internal force increased the rigidity of the manipulator.

## IV. IMPROVEMENT OF THE KINEMATIC MODEL

From the result of accuracy test, a high repeat accuracy was observed, however, the absolute position error was large. For improving the absolute position accuracy, further analysis and experiments were conducted.

### A. Deformation of the springs

As an unique characteristic of the manipulator, the structure is composed by spring elements. The deformation of the springs is assumed as a circular arc (length of  $L_a$  and side length of  $R + D$ ) in the kinematic model. However, in the case, where the deformation is not precisely match on the kinematic model, it can be a cause of the absolute position error. Therefore, the deformation of springs in a bending motion was measured by using a 2D laser displacement meter (LJ-G080, Keyence Inc.). The experimental result in a bending motion of 30 deg is shown in Fig.11. From this

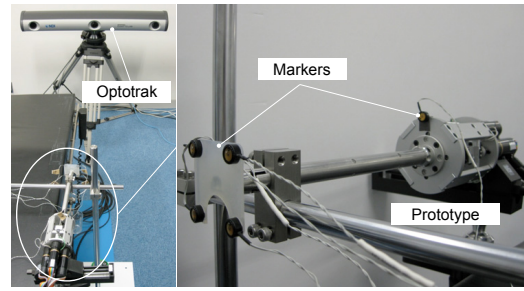


Fig. 8. Setup of 3D position measurement system

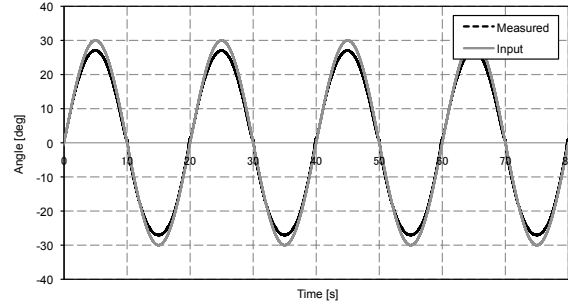


Fig. 9. Experimental result of accuracy test ( $\alpha$  axis)

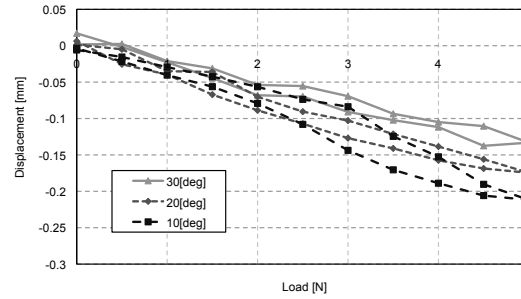


Fig. 10. Experimental result of rigidity test ( $\alpha$  axis)

result, it was observed that the measured bending curve was internally shifted comparing than it was expected in the kinematic model. As the mechanism does not have mechanical constraints to the internal direction, the spring slightly shifted to the internal direction in a bending motion. Therefore, from this measurement, it was assumed that the mismatch between the kinematic model and the actual mechanism occurred. (The other spring in the pair was not measurable because of an occlusion problem of mechanical parts from the laser scan.) From the result of the accuracy test, it was observed that the bending angle of manipulator was smaller than it was expected from the kinematic model. Therefore, it is concerned that this mismatch is related to the absolute position error. Thus, the mismatch have to be compensated for obtaining the further accuracy of manipulator. The error might be removed by introducing an additional mechanical constraints on the springs. However, introducing these additional mechanical components will raise a cost issue on the production processes. In addition, the mechanism will be more complex and may raise the difficulties for a further miniaturization of the structure. Therefore, we propose a method for improving the accuracy of manipulator by optimizing a mechanical parameter in the kinematic model.

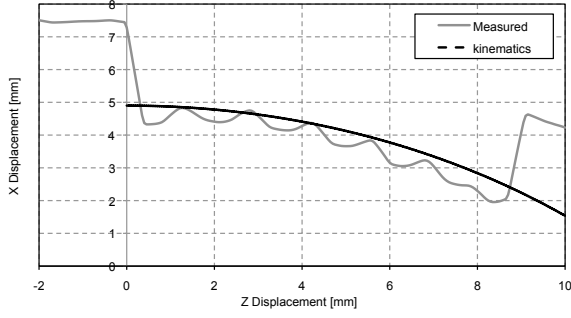


Fig. 11. Experimental result of 2D laser displacement measurement

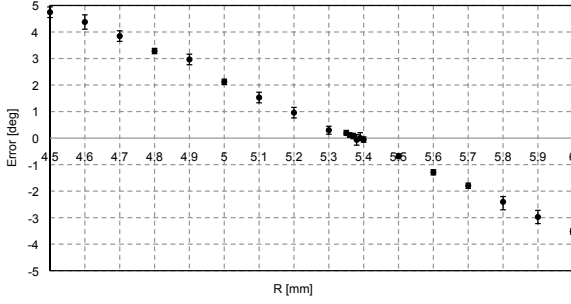


Fig. 13. Position error in varying  $R$

### B. Improvement of accuracy by varying a kinematic parameter

The deformation of springs in the kinematic model are given by the following equation:

$$(X - D)^2 + Z^2 = (R + D)^2 \quad (10)$$

$(P_X, P_Y, P_Z)$  is the coordinates of a tip of spring, which can be determined by the bending angles  $\alpha$  and  $\beta$ . On the other hand, the following equation can be given from the length of spring  $L_a$  and the side length  $R + D$  for determining the deformation of springs.

$$\frac{\pi}{4}(R + D) = L_a \quad (11)$$

$R$  is an actual mechanical parameter and can not be varied. However, by varying  $R$  in the kinematic model numerically, it is possible to change the deformation of springs as shown in Fig.12. The mechanical length of  $R$  was originally configured as 4.9 mm in this prototype.

1) *Determination of  $R$* : The absolute position error was measured in varying the kinematic parameter  $R$  in the same manner of the accuracy test (Fig.13).  $R$  was varied from 4.5 to 6.0 mm, and the error was measured on the peak of trajectory. From this result, the optimal  $R$  was 5.39 mm. By configuring  $R$  as 5.39 mm, the absolute position error decreased down to 0.05 deg in average. By this experiment, it was observed that the absolute position error was drastically improved by determining the optimal  $R$ . A comparison of the trajectory between  $R = 4.9$  mm and  $R = 5.39$  mm was illustrated in Fig.14.

2) *Estimation of  $R$* : From the section B.1) in this chapter, it was shown that the accuracy can be improved by optimizing a kinematic parameter. Therefore, the additional

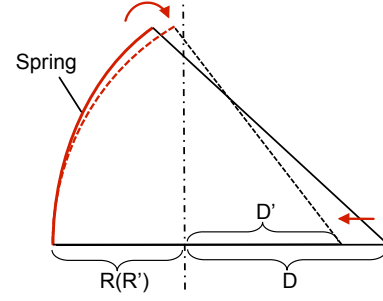


Fig. 12. Improvement of accuracy by varying the kinematic parameter  $R$

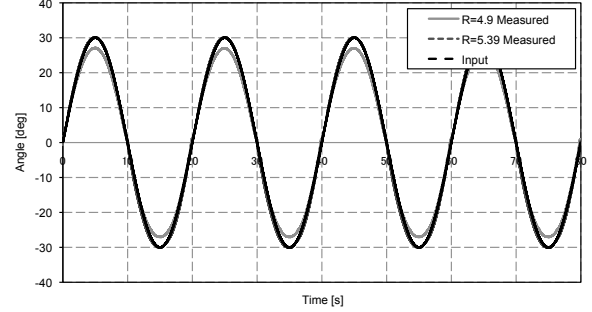


Fig. 14. Trajectory of manipulator in varying  $R$

TABLE III  
POSITION ERROR OF MOTIONS IN  $\alpha$  AXIS

Angle [deg]	Non-compensated [deg]		Compensated [deg]	
	Average	SD	Average	SD
10	0.018	0.039	0.093	0.012
20	0.588	0.159	-0.113	0.033
30	2.280	0.124	-0.050	0.070

experiments were conducted in different trajectories for adopting this optimization method to a free-motion, for such a master-slave control. As the position order, the sine curve was used as well as the previous experiment. The amplitude was set as  $\pm 20$  and  $\pm 10$  deg, the cycle time was set as 20 s. The optimal  $R$  of each trajectory was determined by the same manner introduced in the section B.1) in this chapter. From the experimental result, the improvement of accuracy was observed by introducing the compensation method. It was shown that the effect of the compensation was clearly shown in a larger bending angle (Table III). In addition, it was observed that the optimal kinematic parameter  $R$  lineally changes depending on the target position (Fig.15). From these results, it is suggested that the accuracy can be improved by changing the kinematic parameter  $R$  adaptively in a free-motion.

Fig.16 shows the experimental result of free-motion. A position order of a single bending motion ( $\alpha$  axis) was given by a master device, which was operated by a free hand motion. Then, the manipulator followed the position order in real-time as a slave robot. The absolute position error measured in a same manner with the accuracy test was 0.015 deg in average. Thus, the advantage of the proposed method was clearly shown in this experiment.

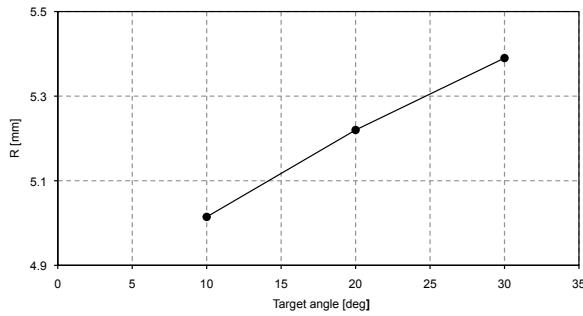


Fig. 15. Estimation of  $R$

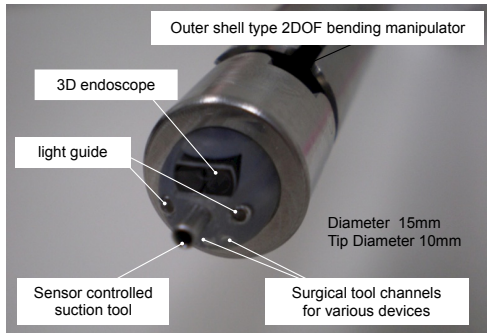


Fig. 17. Implementation of the outer shell type 2 DOF bending manipulator in a neurosurgical application

## V. CONCLUSIONS

In this paper, the outer shell type 2 DOF bending manipulator using spring-link mechanism is presented. As a unique characteristic of the manipulator, the structure is composed by spring elements, and these spring elements are interconnected. From the evaluation tests, it was shown that the manipulator has high rigidity and repeat accuracy. In addition, a method of accuracy improvement was presented in this paper. From the evaluation test, it was observed that the absolute position accuracy was drastically improved on a single bending motion. Therefore, the presented error compensation method showed an advantage of the manipulator. Introducing the presented method to a multi-DOF bending motion is currently on-going work. A high accuracy manipulator such we presented in this paper can be beneficial, especially on image-guided surgical applications. An implementation of the manipulator as a multi-tool equipped surgical tool (Fig.17) is also on-going work.

Comparing with a wire mechanism, the presented mechanism showed an advantage on accuracy, as it does not have drawbacks on frictions and extensions on its power transmissions. On the other hand, comparing with a link mechanism, the manipulator has relatively a simple mechanism, and realized an internal cavity in the structure by introducing the elastic mechanism around the manipulator. In addition, the presented mechanism realizes backlash-free motions for further accuracy. In further development of the manipulator, a repeat durability test is required to clarify the advantages of the proposed manipulator. In addition, an implementation method for more miniaturized mechanism based on the presented manipulator is currently under development.

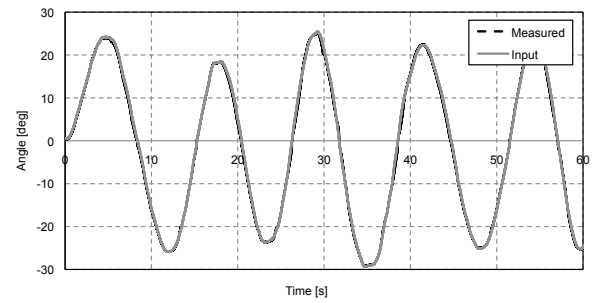


Fig. 16. Trajectory of a free-motion in optimal  $R$

## VI. ACKNOWLEDGMENTS

A part of this study was funded by NEDO P08006 “Intelligent Surgical Instruments Project”, Japan.

## REFERENCES

- [1] PP Pott, HP Scharf, MLR Schwarz, “Today’s state of the art in surgical robotics,” *Computer Aided Surgery*, vol.10-2, pp.101-132, 2005.
- [2] GS Guthert, JK Salisbury, “The Intuitive Telesurgery System: Overview and Application,” *Proc. of Int. Conf. on Robotics and Automation*, pp.618-621, April 2000.
- [3] K Ikuta, K Yamamoto, K Sasaki, “Development of Remote Microsurgery Robot and New Surgical Procedure for Deep and Narrow Space,” *Proc. of IEEE Int. Conf. on Robotics and Automation*, pp.1103-1108, 2003.
- [4] P Dario, MC Carrozza, M Marcacci, S D’Atanasio, B Magnani, O Tonet, G Megali, “A Novel Mechatronic Tool for Computer-Assisted Arthroscopy,” *IEEE Trans. on Information Tech. in Biomedicine*, Vol.4, No.1, pp.15-29, 2000.
- [5] K Harada, Z Bo, S Enosawa, T Chiba, MG Fujie, “Bending Laser Manipulator for Intrauterine Surgery and Viscoelastic Model of Fetal Rat Tissue,” *Proc. of IEEE Int. Conf. on Robotics and Automation*, pp.611-616, 2007.
- [6] J Peirs, D Reynaerts, HV Brussel, GD Gersem, HW Tang, “Design of an advanced tool guiding system for robotic surgery,” *Proc. of IEEE Int. Conf. on Robotics and Automation*, pp.2651-2656, 2003.
- [7] U Seibold, B Kübler, G Hirzinger, “Prototype of Instrument for Minimally Invasive Surgery with 6-Axis Force Sensing Capability,” *Proc. of IEEE Int. Conf. on Robotics and Automation*, pp.498-503, 2005.
- [8] K Xu, N Simaan, “Actuation Compensation for Flexible Surgical Snake-like Robots with Redundant Remote Actuation,” *Proc. of the IEEE Int. Conf. on Robotics and Automation*, pp.4148-4154, 2006.
- [9] M Hashizume, T Yasunaga, K Tanoue, S Ieiri, K Konishi, K Kishi, H Nakamoto, D Ikeda, I Sakuma MG Fujie, T Dohi, “New real-time MR Image-guided Surgical Robotic System for Minimally Invasive Precision Surgery,” *Int. Journal of Computer Assisted Radiology and Surgery*, Vol. 2, pp.317-325, 2008.
- [10] T Kawai, K Kan, K Hongo, K Nishizawa, F Tajima, MG Fujie, T Dohi, K Takakura, “Bipolar coagulation - capable microforceps,” *IEEE Engineering in Medicine and Biology Magazine*, Vol.24, Issue 4, pp.57-62, 2005.
- [11] FV Meer, A Giraud, D Esteve, X Dollat, “A Disposable Plastic Compact Wrist for Smart Minimally Invasive Surgical Tools,” *Proc. of IEEE/RSJ Int. Conf. of Intelligent Robots And Systems*, *Intelligent Robots and Systems*, pp.3051-3056, 2005.
- [12] D Azuma, J Lee, K Narumi, F Arai, “Fabrication and Feedback Control of an Articulated Microarm,” *Proc. of IEEE Int. Conf. on Robotics and Automation*, pp.3073-3078, 2009.
- [13] JP Merlet, “Optimal design for the micro parallel robot MIPS,” *Proc. of IEEE Int. Conf. on Robotics and Automation*, pp.1149-1154, 2002.
- [14] H Yamashita, D KIM, N Hata, T Dohi, “Multi-Slider Linkage Mechanism for Endoscopic Forceps Manipulator,” *Proc. of IEEE/RSJ Intl. Conf. on Intelligent Robots and Systems*, pp.2577-2582, 2003.
- [15] J Arata, M Mitsubishi, S Warisawa, K Tanaka, T Yoshizawa, M Hashizume, “Development of A Dexterous Minimally-Invasive Surgical System with Augmented Force Feedback Capability,” *Proc. of IEEE/RSJ Int. Conf. of Intelligent Robots And Systems*, pp.3738-3743, 2005.